International Journal of Refractory Metals & Hard Materials xxx (xxxx) xxx–xxx

Contents lists available at ScienceDirect

International Journal of Refractory Metals & Hard Materials

journal homepage: www.elsevier.com/locate/IJRMHM

Annealing effect on the fracture toughness of CrN/TiN superlattices

R. Hahn[a,b,*], M. Bartosik[a,b], M. Arndt[c], P. Polcik[d], P.H. Mayrhofer[a,b]

[a] Institute of Materials Science and Technology, TU Wien, 1060 Vienna, Austria
[b] Christian Doppler Laboratory for Application Oriented Coating Development at the Institute of Materials Science and Technology, TU Wien, 1060 Vienna, Austria
[c] Oerlikon Balzers, Oerlikon Surface Solutions AG, Liechtenstein
[d] Plansee Composite Materials GmbH, Lechbruck am See, Germany

ARTICLE INFO

Keywords:
Hard coatings
Superlattice
Fracture toughness
Micromechanical testing
Annealing effect

ABSTRACT

Superlattice films are generally known for their exceptional high hardness compared to their monolithic constituents. Recently, we have shown that CrN/TiN superlattice films exhibit a peak in fracture toughness for a bilayer period of 6.0 nm, similar to the former reported peak in hardness. We propose that a dominating factor for obtaining such favourable material properties is the interface constitution between the individual layers.

To proof this notion, we have intentionally modified the interface sharpness by post-deposition vacuum annealing of the samples at different temperatures. This promotes interdiffusion of Ti or Cr into its adjacent layers and gradually changes the interfaces to interphases (because TiN and CrN form a solid solution). In order to obtain reliable K_{IC} fracture toughness values as a function of the annealing temperature, in-situ micromechanical cantilever bending tests on ex-situ vacuum annealed freestanding films were performed. High temperature loads take also place during machining processes like dry cutting or high-speed cutting, and are thus of high practical relevance.

1. Introduction

In machining industry, polycrystalline ceramic materials with enhanced mechanical and chemical properties are used as protective coatings on drill bits or insert tips for example. These hard coatings protect the underlying tool-materials from severe loads and harmful environmental conditions prolonging the lifetime of the whole tool system [1]. One of the emphases in this field of materials science is to further improve the coating performance by growing the films in a nanolayered architecture [2]. Recently, we have shown that nanolayered thin films, composed of two coherently stacked materials (referred as superlattice systems), exhibit a peak in fracture toughness (K_{IC}) vs. the bilayer period (Λ), similar to the well-known hardness (H) peak [3]. The fracture toughness of hard coatings is crucial to ensure safe operation and to prolong the lifetime of the coated tool [4]. Other strategies to enhance the fracture toughness of hard coatings comprise toughening by incorporating a ductile phase [5,6], microstructural toughening by depositing nanocrystalline materials [7,8], introduction of compressive stresses [9], or phase transformation toughening [10]. Such findings often widen the field of application for hard coating material systems.

Besides these favourable properties in the as-deposited state, protective coatings also have to meet these requirements at elevated temperatures, present during machining processes for example. These operating conditions lead to a possible high temperature-oxidation or undesired recrystallization of a certain microstructure or, as particular interesting for our case, to intermixing of the distinctive nanolayers. Such processes typically limit the operation time of the whole tool system [11–14].

To assess the influence of high temperatures on the mechanical properties of superlattice coatings, two different CrN/TiN multilayers (with bilayer periods Λ of 9 nm and 18 nm) were vacuum annealed up to temperatures of 800 °C. Afterwards, in-situ micro-fracture experiments on freestanding film material, from which pre-notched μ-beams were prepared by Focused Ion Beam (FIB) milling, were conducted. These cantilevers were loaded by a PicoIndenter until fracture. From the maximum force at fracture and by taking into account the actual beam and pre-notch dimensions, the fracture toughness is evaluated for the annealed coatings. These results are also correlated with the hardness evolution with temperature.

2. Experimental

Our CrN/TiN superlattice coatings were deposited with an AJA Orion 5 lab-scaled PVD deposition plant equipped with one three-inch Ti and one two-inch Cr target (99.6% purity, Plansee Composite

* Corresponding author at: Institute of Materials Science and Technology, TU Wien, 1060 Vienna, Austria.
E-mail address: rainer.hahn@tuwien.ac.at (R. Hahn).

https://doi.org/10.1016/j.ijrmhm.2017.11.008
Received 9 October 2017; Accepted 7 November 2017

Materials GmbH). In the unbalanced reactive magnetron sputtering process, the cathodes were DC powered using a power density of 11.0 W/cm^2 and 12.3 W/cm^2 for the Ti and Cr target, respectively. The base pressure of the deposition plant was below 2*10^{-4} Pa. Prior to the deposition, the substrates (single crystalline Al_2O_3 (1–102), 10 × 10 × 0.5 mm^3) were ultrasonically cleaned in acetone and ethanol for 5 min each, mounted inside the chamber and thermally cleaned for 20 min (at 500 °C). Subsequent, the substrates were further cleaned by plasma etching for 10 min using Ar^+ ions by applying a voltage of − 750 V in Ar atmosphere at a total pressure of 6 Pa.

The deposition itself was carried out at a substrate temperature of 500 °C and an Ar/N_2 mixture (5 sccm each) with a total pressure of 0.4 Pa. In order to achieve a dense film growth morphology, a bias voltage of − 60 V (DC) was applied to the rotating substrates [15]. The multilayer architecture was realized using a computer controlled shutter system (the shutters are mounted in front of the targets). All of our thin films are equally thick (~2 μm) and have bilayer periods Λ of 1.8, 4.0, 9.0, 13.2, 18.0 and 186 nm (symmetrically composed of TiN and CrN layers). These bilayer periods are obtained by dividing the total film thickness with the total number of CrN-TiN bilayers, which are in excellent agreement with measured bilayer periods using transmission electron microscopy, as shown in Ref. 3.

The specimens with a bilayer period Λ of 9.0 and 18.0 nm were vacuum annealed at temperatures of 600, 700, and 800 °C with a holding time at the peak temperature of 30 min using a heating rate to this temperature of 20 K min^{-1} (within an CENTORR LF22-2000 Series Vacuum furnace). After annealing, the specimens were passively cooled down to room temperature by turning off the heater (thereby the cooling rate was > 50 K min^{-1} for temperatures above 400 °C).

The X-ray diffraction patterns were collected in symmetric Bragg-Brentano geometry using a PANalytical XPert Pro MPD (θ-θ diffractometer) equipped with a Cu K_α X-ray radiation source (λ = 1.540562 Å).

A Fischer Cripps Laboratories ultra-micro indentation system (UMIS) equipped with a Berkovich diamond tip was used to evaluate the hardnesses of our coatings. Therefore, a series of indentations with different normal loads was carried out, none of them exceeding an indentation depth > 10% of the total film thickness. The resulting load-displacement curves were analysed using the method of Oliver and Pharr [16].

The fracture toughness was determined by micromechanical single cantilever bending tests of free-cut thin film material. Therefore, the coated Al_2O_3 substrates (as deposited and annealed) were cut into small rectangular pieces (~3 × 4 × 0.5 mm^3) using a water cooled Struers Accutom 50 precision cutter equipped with a diamond cutting blade. The cross section of these platelets was carefully polished using a 1 μm diamond lapping film. Afterwards, these platelets were carefully glued onto a sample-holder in a way that guaranteed a perpendicular alignment of the thin film surface to the indentation axis.

The manufacturing of the cantilevers out of the sample were done by FIB milling using a FEI Quanta 200 3D DualBeam-FIB workstation. The first step was the removal of the Al_2O_3 substrate (see Fig. 1a), which was done by a stepwise milling perpendicular to the film growth direction starting with an acceleration voltage of 30 kV and a milling current of 3.0 nA. The current was reduced to 500 pA for the final milling step near the thin film. Accordingly, the sample holder was tilted 90° and cantilevers with a dimension of ~t × t × 7 t μm^3 were milled out of the freestanding thin film (t denotes the film thickness). These dimensions are based on the guidelines reported by Brinckmann et al. [17]. The initial notch was milled with a current of 50 pA (see Fig. 1b–e).

The in-situ micromechanical experiments were performed in a FEI Quanta 200 FEGSEM scanning electron microscope equipped with a Hysitron PI 85 PicoIndenter. A spherical diamond tip with a tip radius of 1 μm was used. The experiments were carried out in a displacement controlled mode with a nominal displacement rate of 5 nm s^{-1}. For all samples, 5 micro-cantilevers were tested, the average success rate was 70%. During the experiments, the load deflection curves were recorded, showing a linear elastic deformation behaviour of the beams.

The fracture toughness of the thin films was calculated using following formula [18]:

$$K_{IC} = \frac{P_{max} * l}{b * w^{3/2}} * f\left(\frac{a}{w}\right) \quad (1)$$

with

$$f\left(\frac{a}{w}\right) = 1.46 + 24.36 \cdot \left(\frac{a}{w}\right) - 47.21 \cdot \left(\frac{a}{w}\right)^2 + 75.18 \cdot \left(\frac{a}{w}\right)^3 \quad (2)$$

Here, P_{max} denotes the maximum applied load, l the lever arm (between the notch and the position of the indenter), b the width of the cantilever, w the coating thickness (equals the cantilever thickness), and a the initial notch (crack) length (see Fig. 1e).

3. Results

X-ray diffraction patterns, shown in Fig. 2, reveal a face-centered cubic (c) structure of all our thin films. Cumulative main peaks are between the expected peak positions of c-TiN and c-CrN. Additional positive and negative satellite peaks are present for the coatings with bilayer periods of 9.0, 13.2, and 18.0 nm. Both characteristics, cumulative peaks in between the peak position of the constituents and the presence of satellite peaks, reveal the existence of a superlattice structure [19]. Consequently, the superlattice structure is absent (or at least not pronounced) for the films with a nominal bilayer period of 1.8, 4.0, and 186 nm. We expect a solid solution of TiN and CrN for the coatings with Λ = 1.8 and 4.0 nm, due to their thermodynamically complete miscibility and the conditions used during deposition. For the film with the largest bilayer period (Λ = 186 nm), clearly individual peaks for c-TiN and c-CrN can be detected, suggesting a mainly independent growth of c-TiN and c-CrN layers. The crystal structure of the sapphire substrate used (which is hexagonal) promotes a polycrystalline growth structure of our cubic structured coatings.

Already after annealing at 600 °C, the XRD peak positions clearly shifted to higher diffraction angles (see our examples with Λ = 9.0 and 18.0 nm as a function of annealing temperature T_a, insets on the right side of Fig. 2). This suggests for pronounced recovery-effects of built-in structural defects during the annealing treatment. Furthermore, also the intensity of the satellite peaks decreases with T_a (clearly observable for the Λ = 18.0 nm sample). But also the sample with smaller bilayer period (Λ = 9.0 nm) shows a significant change of the XRD shape with T_a. These changes in XRD patterns suggest that both samples experience significant structural modifications (e.g., interdiffusion of the TiN and CrN layers, recovery of structural and superlattice effects) due to the annealing treatment up to 800 °C.

The as deposited hardness measurements versus the bilayer period, Fig. 3a, reveal a behaviour typical for superlattice structures [20,21]. The hardness initially increases with decreasing bilayer period according to a Hall-Petch-like effect [3]. Then, with Λ = 9.0 nm, the hardness peaks and with even smaller bilayer periods, the hardness decreases again. Chu and Barnett proposed two main mechanisms to be responsible for this effect [22]. For small bilayer periods (hence, the left side of the hardness peak in our Fig. 3), the stress required for a dislocation to propagate across the interface between layers (with different shear moduli) increases with increasing bilayer period. Thereby the determining, materials-related effects are the repulsion of dislocations due to a difference in the shear moduli of adjacent layers. These effects change with the bilayer period and the composition modulation (i.e., the interface sharpness). This mechanism is limited by the second mechanism, the Hall-Petch effect, where interfaces impede dislocations to traverse from grain to grain (or here layer to layer). Hence, with decreasing bilayer period the number of pinning points (i.e., the interfaces) impeding dislocation movements increases, leading to an

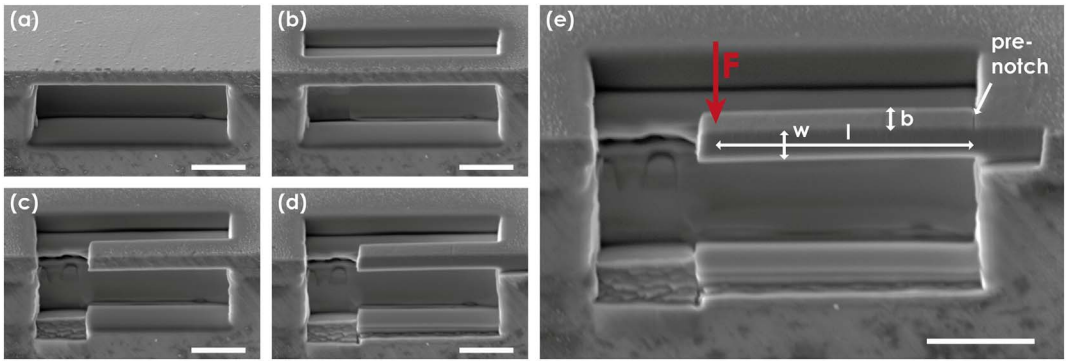

Fig. 1. (a)–(e) SEM images showing the milling steps of our cantilevers (inclined by 52°). The brighter appearance of the thin film surface in (a) results from the necessary 4 nm Au-Pd coating (otherwise the drift due to the poor conductivity would be too high for precise FIB-milling). The Au-Pd is removed step by step due to ion-images taken between the milling steps and limitations in the precision of the Ga^+-ion gun. Image (e) additionally shows the dimensions of the cantilever used to calculate the fracture toughness and the initial notch (the initial notch depth is not shown here). The scale bars are 5 μm in size.

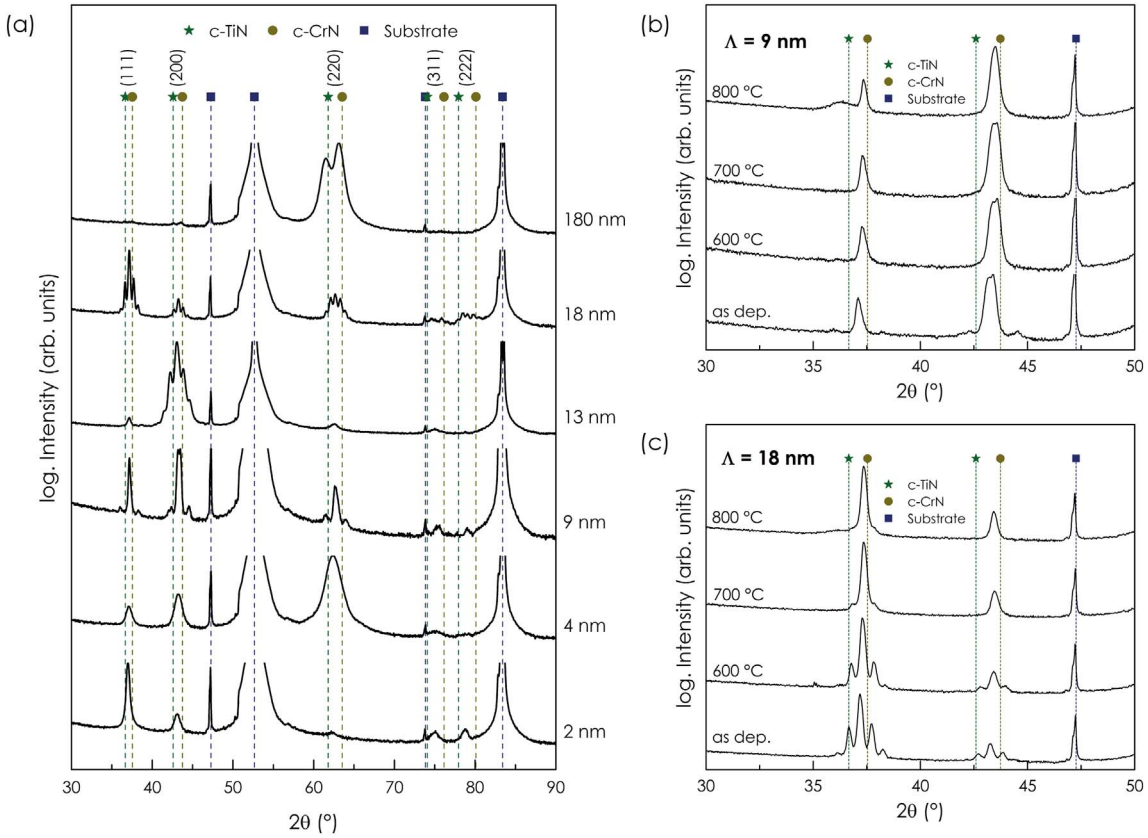

Fig. 2. (a) shows XRD patterns of CrN/TiN superlattice thin films with differing bilayer periods Λ (186, 18.0, 13.2, 9.0, 4.0, and 1.8 nm from top to bottom) in the as deposited state. (b) and (c) show XRD patterns of annealed samples with Λ = 9.0 and 18.0 nm respectively.

increased strengthening. The combination of both effects lead to the observed hardness peak or an optimum bilayer period Λ. As reported by Chu and Barnett, the hardness enhancement in these multilayered system is a plasticity driven phenomenon and thus characterized by inhibited dislocation movement. The peak hardness of 28.4 ± 0.8 GPa for our CrN/TiN superlattice film with Λ = 9.0 nm exceeds the hardness of their single layered constituents (H_{CrN} = 20.3 ± 0.9 GPa and H_{TiN} = 28.1 ± 0.9 GPa, when prepared with the same deposition conditions).

The hardness of our samples steadily decreases with increasing annealing temperature, Fig. 3b. This decrease is most pronounced for the sample with Λ = 9.0 nm (i.e., the coating with the peak hardness due to the superlattice effect), especially between 500 and 600 °C. Based on the quasibinary phase diagram between CrN and TiN – which suggests full solubility along the entire composition range – we conclude that this is mainly based on interdiffusion between the CrN and TiN layers. The reduction in hardness by ~3.8 GPa – from H = 28.4 ± 0.8 to 24.6 ± 0.9 GPa – is nearly the gain in hardness due to the superlattice effect, hence the difference between the coating exhibiting the as deposited peak hardness and the coatings without a superlattice structure, see Fig. 3a and Ref. 3. As mentioned above, the superlattice effect is (amongst others) based on impeded dislocation movements across interfaces, which is reduced by interdiffusion processes, especially if the individual layers are thin enough and allow a complete transformation into a solid solution. The other sample, with larger bilayer period (Λ = 18.0 nm) also exhibits a hardness decrease with T_a. But the hardness reduction from 24.2 ± 0.9 to 22.6 ± 0.8 upon annealing to 600 °C is significantly less pronounced, and

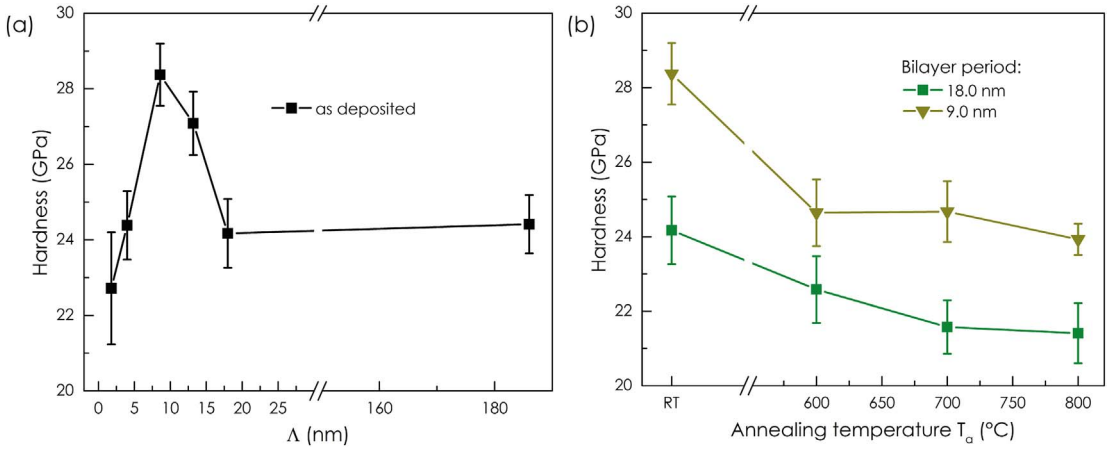

Fig. 3. (a) Hardness H versus bilayer period Λ of our CrN/TiN superlattice coatings on Al_2O_3 (1–102) substrates. The peak in H vs. Λ is typical and characteristic for superlattice thin films. (b) Hardness versus annealing temperature T_a of the superlattice coating with the hardness peak (Λ = 9.0 nm) and one with significantly larger bilayer period (Λ = 18.0 nm). The hardness value for T_a = 500 °C represents the as deposited hardness, because the deposition temperature was 500 °C.

corresponds presumably to recovery-induced effects. Here, no significant superlattice effect is reduced, because the bilayer period was beyond the needed value for peak-hardness, compare Fig. 3a and b.

Based on the superlattice effect, the as deposited fracture toughness (in addition to the hardness) is higher for the Λ = 9.0 nm sample (K_{IC} = 2.3 ± 0.15 MPa√m) than for the Λ = 18.0 nm sample (K_{IC} = 1.7 ± 0.14 MPa√m), Fig. 4, which was reported in detail in Ref. 3. But contrary to the hardness development, the fracture toughness shows a different behaviour with annealing temperature for these samples. The fracture toughness of the Λ = 9.0 nm sample decreases from 2.3 ± 0.15 MPa√m to 1.8 ± 0.19 MPa√m upon annealing at 600, 700, and 800 °C. This reduction in fracture toughness by ~0.5 MPa√m is almost the gain due to the superlattice effect, described in Ref. 3, and the difference between the as deposited samples with Λ = 9.0 and 18.0 nm. Interestingly, the sample with the larger bilayer period (Λ = 18.0 nm), hence the sample without a significant superlattice effect in hardness and/or fracture toughness, shows a nearly opposite behaviour, where K_{IC} initially increases with annealing temperature, Fig. 4. The highest fracture toughness for this sample is 2.2 ± 0.12 MPa√m and obtained after annealing at 700 °C. When annealed at even higher temperatures (800 °C), the fracture toughness only slightly decreases to 2.1 ± 0.11 MPa√m, see Fig. 4.

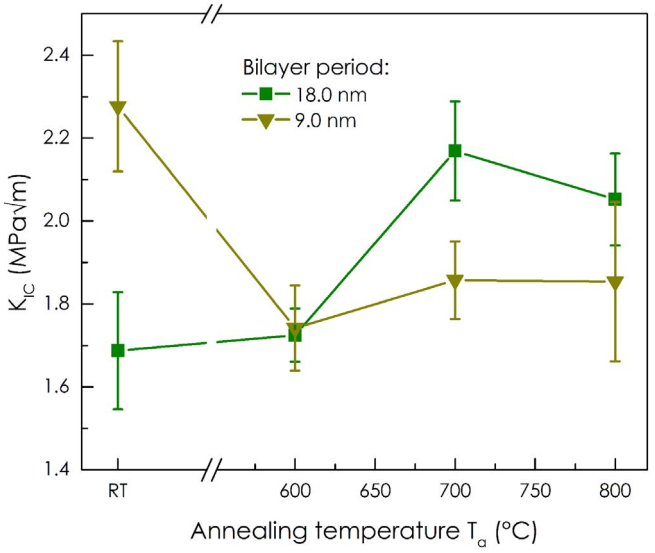

Fig. 4. Fracture toughness K_{IC} as a function of the annealing temperature T_a for the samples with a bilayer period Λ of 9.0 and 18.0 nm.

4. Discussion

The different behaviour of hardness H and fracture toughness K_{IC} upon annealing is not fully understood and needs further (more detailed) investigations, by high resolution transmission electron microscopy studies for example. However, here we want to discuss possible reasons why H decreases but K_{IC} increases, especially for the sample with a large bilayer period Λ of 18.0 nm.

The reduction in H upon annealing to temperatures above the deposition temperature of 500 °C follows the trend for single-phased binary PVD coatings, especially if no decomposition or precipitation takes place [23–25]. The reduction in hardness upon annealing is basically driven by the reduction of structural built-in defects (due to the deposition process) or their rearrangement to lower energy configurations and sites (i.e., recovery processes). The sample with a bilayer period Λ of 9.0 nm, which shows the highest hardness (due to the most pronounced superlattice effect), also exhibits the highest hardness reduction upon annealing. The results suggest that already after annealing at 600 °C a significant contribution to the superlattice effect is eliminated (because here, the hardness value with 24.6 ± 0.9 GPa corresponds to those of the as deposited samples without significant superlattice effect). In addition to the mentioned recovery effects, also interdiffusion of the adjacent TiN and CrN layers will take place during annealing, because (as mentioned above) TiN and CrN show a full miscibility along the entire composition range - also because of their very similar structure (B1, face centered cubic) and lattice parameters of 4.2417 Å (PDF 00-038-1420 (ICDD, 1987)) and 4.140 Å (PDF 00-011-0065 (ICDD, 1958)), respectively. Due to the interdiffusion of the adjacent TiN and CrN layers, the superlattice structure will be eliminated (or at least reduced) if the layers are thin enough. Furthermore, the XRD data suggest (based on the integral width of the (111) XRD peaks) that the coherently scattering domain size increases (from ~ 35 to 54 nm) upon annealing this sample with Λ = 9.0 nm.

The sample with a bilayer period Λ of 18.0 nm, hence without a significant superlattice contribution to the hardness, also experiences a hardness reduction upon annealing (due to recovery effects). But here, the reduction is not that pronounced as for the other sample with Λ = 9.0 nm. Furthermore, here the XRD data suggests actually decreasing coherently scattering domain sizes (from ~ 74 to 63 nm) with increasing annealing temperature. We envision that this is based on interdiffusion between the adjacent TiN and CrN layers. As these are rather thick for this sample (with 9 nm in the as deposited state), not the entire layer thickness is consumed by interdiffusion (as obtained for the sample with Λ = 9.0 nm) and a multiphased layer arrangement of TiN, $Ti_{1-x}Cr_xN$ and CrN can form. However, the reduction in domain

size cannot counteract for the recovery-induced hardness reduction.

Especially the different interdiffusion stages of the samples can be a reason for the observed different behaviour of their fracture toughness upon annealing. For the sample with $\Lambda = 9.0$ nm, XRD suggests for increasing domain sizes and loss of superlattice structure with increasing T_a. In combination with the transformation towards a $Ti_{1-x}Cr_xN$ solid solution (as the adjacent TiN and CrN layers are thin enough), this can explain their reduction in fracture toughness upon annealing. Contrary, the newly formed multiphased layer arrangement of the sample with $\Lambda = 18.0$ nm (here, the individual TiN and CrN layers are twice as thick as for the other sample and thus not fully transformed towards a $Ti_{1-x}Cr_xN$ solid solution upon interdiffusion) in combination with the thereby associated decreasing domain size with increasing T_a, can be responsible for the observed increase in fracture toughness.

5. Summary and conclusion

As elevated temperatures are present during many industrial applications, we studied the influence of annealing temperatures T_a on mechanical properties of CrN/TiN superlattice coatings, with a focus on their fracture toughness. In the as deposited state, hardness H as well as fracture toughness K_{IC} show a comparable dependence on the bilayer period, with peaks at $\Lambda = 9.0$ nm for H (28.4 ± 0.8 GPa) and K_{IC} (2.3 ± 0.15 MPa√m). As expected for coatings without decomposition processes, the hardness decreases with increasing annealing temperature T_a. The $\Lambda = 9.0$ nm superlattice coating with the as deposited peak hardness, exhibits a significant hardness decrease to 24.6 ± 0.9 GPa, already when annealed at 600 °C – due to structural recovery effects and interdiffusion between the adjacent TiN and CrN layers. The coating with a large bilayer period of $\Lambda = 18.0$ nm (having no significant superlattice effect in the as deposited state), only experiences a hardness reduction from 24.2 ± 0.9 to 22.6 ± 0.8 GPa with increasing T_a to 600 °C.

Contrary to this behaviour, the K_{IC} vs. T_a dependence is different for the coatings with $\Lambda = 9.0$ or 18.0 nm. The coating with a bilayer period Λ of 9.0 nm (having the peak in K_{IC} with 2.3 ± 0.15 MPa√m) experiences a reduction in K_{IC} to 1.8 ± 0.19 MPa√m due to annealing at $T_a = 600$, 700 and 800 °C. However, the coating with a bilayer period of $\Lambda = 18.0$ nm, exhibits even an increase in K_{IC} from 1.7 ± 0.14 MPa√m to 2.2 ± 0.12 MPa√m when annealed at $T_a = 700$ °C. This coating – contrary to the coating with $\Lambda = 9.0$ nm, which exhibits a significant superlattice effect – experiences a reduction in coherently diffracting domain size due to annealing. We envision that the larger bilayer period allows for a TiN/CrN interdiffusion based formation of a multiphased layered arrangement (with smaller domain sizes), leading to an improvement in K_{IC} upon annealing.

Based on our findings we can conclude that the fracture toughness can show a different (even opposite) dependence on annealing treatments (or exposure to elevated temperatures) than the hardness. This is of utmost importance as many applications will lead to an annealing treatment of the coatings used, and both properties – hardness and fracture toughness – are at least equally important.

Acknowledgements

The financial support by the Austrian Federal Ministry of Economy, Family and Youth and the National Foundation for Research, Technology and Development is greatly acknowledged. We also thank Oerlikon Balzers, Oerlikon Balzers Surface Solutions AG and Plansee Composite Materials GmbH for the financial support. XRD investigations were performed using facilities of the XRC of TU Wien, Austria. FIB and SEM investigation were carried out at the USTEM of TU Wien, Austria. We would also like to thank the Institute for Mechanics of Materials and Structures of TU Wien, Austria for providing the PicoIndenter.

References

[1] P.H. Mayrhofer, A. Hörling, L. Karlsson, J. Sjölén, T. Larsson, C. Mitterer, L. Hultman, Appl. Phys. Lett. 83 (10) (2003) 2049–2051.
[2] M. Stueber, H. Holleck, H. Leiste, K. Seemann, S. Ulrich, C. Ziebert, J. Alloys Compd. 483 (1–2) (2009) 321–333.
[3] R. Hahn, M. Bartosik, R. Soler, C. Kirchlechner, G. Dehm, P.H. Mayrhofer, Scr. Mater. 124 (2016) 67–70.
[4] S. Zhang, D. Sun, Y. Fu, H. Du, Surf. Coat. Technol. 198 (1–3) (2005) 2–8.
[5] J. Musil, P. Zeman, H. Hrubý, P.H. Mayrhofer, Surf. Coat. Technol. 120–121 (1999) 179–183.
[6] M. Mišina, J. Musil, S. Kadlec, Surf. Coat. Technol. 110 (3) (1998) 168–172.
[7] S. Veprek, A. Niederhofer, K. Moto, T. Bolom, H.-D. Männling, P. Nesladek, G. Dollinger, A. Bergmaier, Surf. Coat. Technol. 133–134 (2000) 152–159.
[8] S. Veprek, M. Haussmann, S. Reiprich, J. Vac. Sci. Technol. A 14 (1995) 46–51.
[9] S. Hogmark, S. Jacobson, M. Larsson, Wear 246 (1–2) (2000) 20–33.
[10] M. Schlögl, C. Kirchlechner, J. Paulitsch, J. Keckes, P.H. Mayrhofer, Scr. Mater. 68 (12) (2013) 917–920.
[11] W.D. Münz, J. Vac. Sci. Technol. A 4 (6) (1986) 2717–2725.
[12] H. Riedl, D. Holec, R. Rachbauer, P. Polcik, R. Hollerweger, J. Paulitsch, P.H. Mayrhofer, Surf. Coat. Technol. 235 (2013) 174–180.
[13] H.C. Barshilia, A. Jain, K.S. Rajam, Vacuum 72 (3) (2003) 241–248.
[14] M. Schlögl, J. Paulitsch, P.H. Mayrhofer, Surf. Coat. Technol. 240 (2014) 250–254.
[15] P.H. Mayrhofer, C. Mitterer, L. Hultman, H. Clemens, Prog. Mater. Sci. 51 (8) (2006) 1032–1114.
[16] W.C. Oliver, G.M. Pharr, J. Mater. Res. 7 (6) (1992) 1564–1583.
[17] S. Brinckmann, C. Kirchlechner, G. Dehm, Scr. Mater. 127 (2017) 76–78.
[18] K. Matoy, H. Schönherr, T. Detzel, T. Schöberl, R. Pippan, C. Motz, G. Dehm, Thin Solid Films 518 (1) (2009) 247–256.
[19] C.H. Johannson, J.O. Linde, Ann. Phys. 383 (21) (1925) 439–460.
[20] U. Helmersson, S. Todorova, S.A. Barnett, J.-E. Sundgren, L.C. Markert, J.E. Greene, J. Appl. Phys. 62 (2) (1987) 481–484.
[21] H.C. Barshilia, K.S. Rajam, Bull. Mater. Sci. 26 (2) (2003) 233–237.
[22] X. Chu, S.A. Barnett, J. Appl. Phys. 77 (9) (1995) 4403–4411.
[23] P.H. Mayrhofer, F. Kunc, J. Musil, C. Mitterer, Thin Solid Films 415 (1–2) (2002) 151–159.
[24] P.H. Mayrhofer, G. Tischler, C. Mitterer, Surf. Coat. Technol. 142–144 (2001) 78–84.
[25] C. Mitterer, P.H. Mayrhofer, J. Musil, Vacuum 71 (1–2) (2003) 279–284.